

## Coarse-graining scheme for simulating uniaxial stress-strain response of glassy polymers through molecular dynamics

Manoj K. Majumder, Ramkumar S., Dhiraj K. Mahajan, and Sumit Basu\*

*Department of Mechanical Engineering, Indian Institute of Technology Kanpur, Kanpur, Uttar Pradesh 208016, India*

(Received 4 September 2009; published 11 January 2010)

Simulation of the deformation of polymers below their glass transition through molecular dynamics provides an useful route to correlate their molecular architecture to deformation behavior. However, present computational capabilities severely restrict the time and length scales that can be simulated when detailed models of these macromolecules are used. Coarse-graining techniques for macromolecular structures intend to make bigger and longer simulations possible by grouping atoms into superatoms and devising ways of determining reasonable force fields for the superatoms in a manner that retains essential macromolecular features relevant to the process under study but jettisons unnecessary details. In this work we systematically develop a coarse-graining scheme aimed at simulating uniaxial stress-strain behavior of polymers below their glass transition. The scheme involves a two step process of obtaining the coarse grained force field parameters above glass transition. This seems to be enough to obtain “faithful” stress-strain responses after quenching to below the glass transition temperature. We apply the scheme developed to a commercially important polymer polystyrene, derive its complete force field parameters and thus demonstrate the effectiveness of the technique.

DOI: [10.1103/PhysRevE.81.011803](https://doi.org/10.1103/PhysRevE.81.011803)

PACS number(s): 82.35.Lr, 83.50.-v, 81.05.Lg, 66.70.Hk

### I. INTRODUCTION

Predicting macroscopic properties of a polymer starting from a description of its molecular architecture is a long standing scientific goal. The problem however, involves a large variety of length and time scales. The range of length scales span a wide spectrum from 0.1 nm which is a typical bond length, to the scale at which typical mechanical tests are conducted, i.e., tens of millimeters. Kuhn lengths for typical polymers are of the order of 1 nm for randomly coiled chains and typical radii of gyration of polymer chains at realistic molecular weights are of the order of 10 nm. Time scales too range from 1 fs, the vibration time period for individual bonds to several seconds, the typical relaxation times for commercial polymers. The fact that the structure and dynamics is governed by such a wide spectrum of time and length scales makes multiscale simulation of these materials especially difficult [1].

Atomistically detailed simulations with a view to obtain macroscopic and in particular, mechanical properties of macromolecular systems have been conducted by several researchers. These include, among others, simulations of stress-strain response of glassy polymers by Brown and Clarke [2], Ogura and Yamamoto [3], Capaldi *et al.* [4], Yashiro *et al.* [5], Negi and Basu [6], and Lyulin *et al.* [7]; viscoelastic properties by Weiner and Gao [8]; adhesive properties by Stevens [9], Rottler and Robbins [10], and Kulmi and Basu [11].

The simulation studies mentioned above use force field models of basically two types. A large body of literature exists on polyethylene (PE)-like models where a “united atom” represents a  $-\text{CH}_2-$  unit, each of which interacts with bond stretching, bending, and torsion potentials with four of its bonded neighbors and through the Lenard Jones (LJ) po-

tential with the rest. The parameters for the force fields are obtained from *ab initio* calculations on *n*-butane as in typical calculations by Steele [12]. Similar models obtained by absorbing the hydrogens into united atoms have been proposed for more complicated molecules like polystyrene [13] and used in molecular dynamics (MD) studies to predict mechanical properties by Lyulin *et al.* [7].

On the other hand, coarse grained simulations involve “beads” that are larger than  $-\text{CH}_2-$  units in size and interact through a force field which is generally taken to be a combination of a finite extensible nonlinear elastic (FENE) potential between adjacent bonds and a truncated and shifted LJ potential. Simulations are often conducted using Lenard Jones units, where the LJ constants are used as reference length and energy scales. Simulations conducted through both routes provide insights into the deformation behavior of these materials. However, unless an equivalence is established between the force field parameters used in united atom and coarse grained (CG) simulation, quantitative comparison of physical quantities obtained from the two methods is difficult.

We illustrate the above point using the example of PE, the simplest linear chain polymer. United atom models of PE use a force field where the total energy of the system is given by

$$E_{UA} = \sum V_{stretch} + \sum V_{bend} + \sum V_{tor} + \sum V_{vdW}, \quad (1)$$

as in Mahajan and Basu [14], where the summations run over all bonds of the particular kind. The van der Waals interactions are calculated over pair of atoms not connected by stretching, bending and torsional potentials. A realistic characterization of the force field for PE assumes (Fukuda and Kuwajima [15]):

$$V_{stretch} = \frac{1}{2}k_s(r - r_0)^2, \quad (2)$$

where  $r_0 = 1.53 \text{ \AA}$  and  $k_s = 2745 \text{ kJ}/(\text{mol } \text{\AA}^2)$ ,

\*sbasu@iitk.ac.in; <http://home.iitk.ac.in/~sbasu>

TABLE I. CG model equivalence with united atom model of PE.

Quantity	Units		CG (LJ)	CG (LJ) $\Rightarrow$ PE (REAL)	PE (REAL)
	LJ	Real	Hoy&Robbins <sup>a</sup>	Kröger <sup>b</sup>	Mahajan and Basu <sup>c</sup>
$a$	$\sigma$	$\text{\AA}$	1	5.23	4.06
$u_o$	$\epsilon$	$\frac{\text{kJ}}{\text{mol}}$	1	3.68	0.36
mass	$m$	$\frac{\text{g}}{\text{mol}}$	1	42.3	14
$r_c$	$\sigma$	$\text{\AA}$	1.5	7.8	6
$R_o$	$\sigma$	$\text{\AA}$	1.5	7.8	
Time step	$\tau_{\text{LJ}}$	ps	0.007–0.012	0.01–0.02	0.002
$T_g$	$\frac{\epsilon}{k_b}$	K	0.35	155	230–260
$\dot{T}$	$\frac{\epsilon}{k_b \tau_{\text{LJ}}}$	$\frac{\text{K}}{\text{ps}}$	$-2 \times 10^{-3}$	-0.5	1.5–0.15
Density	$\frac{m}{\sigma^3}$	$\frac{\text{g}}{\text{cm}^3}$	1	0.49	0.83–0.86
$\Sigma_o$	$\frac{\epsilon}{\sigma^3}$	MPa	1	42.7	210
$\dot{\lambda}$	$\tau_{\text{LJ}}^{-1}$	$\text{ps}^{-1}$	$\approx -10^{-4}$	$\approx -10^{-4}$	$\approx -10^{-4}$
$E$	$\frac{\epsilon}{\sigma^3}$	MPa	15.15	641	2000

<sup>a</sup>Reference [16].<sup>b</sup>Reference [18].<sup>c</sup>Reference [14].

$$V_{\text{bend}} = \frac{1}{2} k_{\theta} [\cos(\theta) - \cos(\theta_0)]^2, \quad (3)$$

where  $k_{\theta} = 749$  kJ/mol and  $\theta_0 = 113.3^\circ$ ,

$$V_{\text{tor}} = \frac{1}{2} A_1 [1 + \cos(\phi)] + \frac{1}{2} A_2 [1 - \cos(2\phi)] + \frac{1}{2} A_3 [1 + \cos(3\phi)], \quad (4)$$

where  $A_1 = 7.86$ ,  $A_2 = -4.36$ , and  $A_3 = 15.56$  kJ/mol,

$$V_{\text{vdW}} = 4\epsilon \left[ \left( \frac{\sigma}{r} \right)^{12} - \left( \frac{\sigma}{r} \right)^6 \right]. \quad (5)$$

where  $\sigma = 4.06$   $\text{\AA}$  and  $\epsilon = 0.36$  kJ/mol.

In the above,  $r$  denotes the distance between two united atoms while  $\theta$  and  $\phi$  are the bond and dihedral angles between three and four consecutive united atoms in a chain.

A coarse grained model on the other hand assumes that adjacent beads interact through the FENE potential as

$$U_{\text{FENE}} = \begin{cases} -\frac{R_o^2 k}{2} \ln[1 - (r/R_o)^2] & r < R_o \\ \infty & r \geq R_o \end{cases},$$

while all bead pairs interact through the truncated and shifted LJ potential as

$$U_{\text{LJ}} = \begin{cases} 4u_o \left[ \left( \frac{a}{r} \right)^{12} - \left( \frac{a}{r} \right)^6 + 1/4 \right] & r < r_c \\ 0 & r \geq r_c \end{cases},$$

where  $r_c = 1.5a$  is the potential cut-off radius (Hoy and Robbins [16]). Thus  $u_o$  becomes a basic unit of energy and “ $a$ ” an unit of length. Further, bending and torsional potentials

may be added to further stiffen the chain (Bulacu and van der Giessen [17]). Kroger [18], comparing the experimental end to end distance of PE chains at temperature of 443 K with CG simulations suggest that  $u_o = 3.68$  kJ/mol and  $a = 5.23$   $\text{\AA}$ . Moreover, the mass of a CG bead is 42.3 g/mol, suggesting that a CG bead is equivalent to about three united atoms.

Based on the above equivalence between the CG and united atom force fields for PE, we have compared key predictions of mechanical properties obtained from them. The comparison is presented in Table I. Clearly, key quantities defining the mechanical behavior for the materials, namely the glass transition temperature  $T_g$ , yield stress  $\Sigma_o$  and the Young’s modulus  $E$  are widely different for the two cases (9th, 12th, and 14th rows in Table. I). This discrepancy points to the need for establishing a closer equivalence between the force field parameters of CG and a united atom model.

The objective of the work is to attempt a related and somewhat more realistic approach to establishing an equivalence between united atom and CG force fields. To this end, we attempt to coarse grain a somewhat more complicated polymer, polystyrene (PS), such that groups of atoms in one or more monomers constituting it are systematically mapped onto *superatoms*, thus reducing significantly the total number of degrees of freedom that need to be accounted for. If efficient strategies for quantifying the interaction between the superatoms can be devised, the process can probably be automated and more importantly, lead to very significant improvements in the time and length scales accessible to MD simulations performed with the coarse grained systems over detailed models. Examples of such attempts to coarse grain particular systems include those by Tschop *et al.* [19], Akkermans and Briels [20], Baschnagel *et al.* [21], Muller-Plathe [22], and the works by Faller and co-workers, especially Sun and Faller [23]. The coarse-grained macro-

molecules are basically linear chains comprised of superatoms interacting through the derived force fields. Ensembles of such chains can then be used in MD simulations with a view to obtaining useful mechanical or other properties. The properties thus derived are essentially “parameter free,” “first principle” estimates.

In the present work our objective is to build and validate a coarse-grained model for PS that is capable of predicting its stress-strain behavior in the glassy state. Polystyrene is a commercially important polymer that exhibits substantial strain softening right after yield (also called a “yield drop”) and moderate strain hardening at large strains [24]. As a consequence, the localization of deformation and the growth of these localized shear bands in polystyrene is significantly different from other commercially important polymers like polycarbonate which have shallower yield drops but harden strongly at high strains [25]. Lyulin *et al.* [7] report a simulation of stress-strain behavior of both polystyrene and polycarbonate that brings out the difference in their strain softening behavior. These simulations use united atom force fields with rather short and few chains. Evidently, an effectively coarse-grained model of polystyrene will allow us to simulate much bigger systems.

An interesting development in this direction has been made by Harmandaris and co-workers [26–30]. Harmandaris *et al.* [29] has performed coarse-graining of polystyrene using two superatoms to represent a monomer of PS. They calibrated the various bond stretching, bending, and dihedral potentials of the coarse-grained model meticulously closely following a procedure that Tschop *et al.* [19] used for coarse graining polycarbonate. In this method, the nonbonded force field is calibrated very accurately while the nonbonded potential (which strongly controls the deformation behavior in the glassy state) is calibrated by, simulating two isolated toluene molecules at various separations, averaging their interaction energies with respect to all orientations and finally fitting a shifted Lennard-Jones potential to the mean-force potential. The calibrated coarse grained force field was used by Mulder *et al.* [27] to generate stress-strain curves for PS in the glassy state.

Molecular dynamics based stress-strain simulations on glassy polymers are typically done on samples which are prepared at high temperatures and then quenched to the glassy state before being deformed. The calibration of the coarse-grained parameters is performed at the high temperature. The coarse-grained model, by design, maintains close equivalence to the corresponding detailed model at the high temperature. Typically, at this temperature, radial distribution functions, structure factors, etc. in the coarse grained system match closely with those of the corresponding detailed system.

However, as has been pointed out by Milano *et al.* [31], the pressure in the coarse-grained model generally does not match that in the detailed model (they proposed to add a weak linear potential to the attractive part of the coarse-grained nonbonded potential to correct for the pressure). Mismatch in pressure at the high temperature implies that the stress after quenching to the glassy state also is different from a detailed sample. Thus a detailed sample equilibrated at above  $T_g$ , quenched to a glassy state and deformed uniaxi-

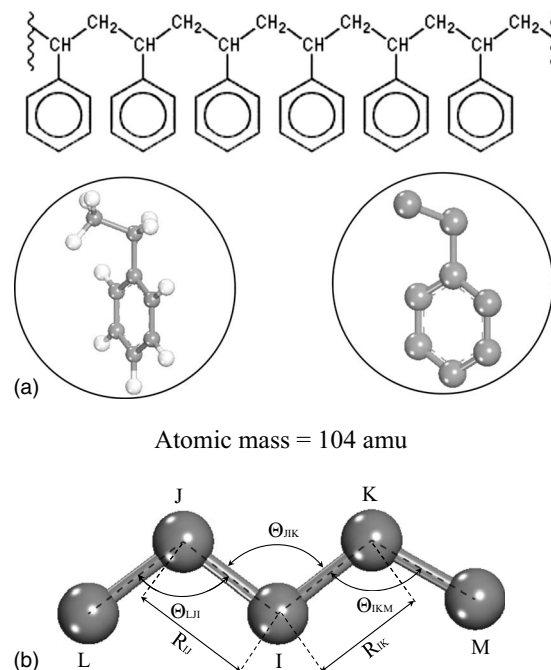


FIG. 1. (a) Chemical structure of the PS molecule along with the optimum structure of its all atom and united atom monomers; (b) Schematic representation of coarse grained PS.

ally, in general, will have a different stress-strain response compared to its coarse grained counterpart quenched and deformed in the same way. This, in our view, is a major bottleneck in coarse graining macromolecules with a view to obtaining their stress-strain behavior in the glassy state. We will show that coarse-graining followed by a pressure correction at the high temperature alleviates this problem to some extent.

The structure of a small part of the polystyrene chain is shown in Fig. 1(a) along with the optimized all atom structure of a monomer and its united atom representation. The optimized structure of a PS monomer is well known, an united atom force field is available in Mondello *et al.* [13] and is briefly described in the next section. In the coarse graining strategy to be adopted here, we will start by taking one superatom per monomer with a mass of 104 amu. So, a macromolecular PS chain, as shown in Fig. 1(b), in the coarse-grained representation is a linear chain of superatoms that are bonded by bond stretching and bending potentials. Moreover, superatoms that do not interact through bonded potentials do so through a nonbonded LJ potential. The basic aim of the coarse-graining (CG) scheme is to calibrate the bonded and nonbonded potentials with a view to matching some physical property of the system, in this case, the stress-strain response in the glassy state.

Several techniques are available for calibrating the CG force field in the literature [19,22,23,32]. Typically, to calibrate the bonded force fields, *ab initio* calculations are conducted on monomers or parts thereof [19]. Moreover, a two-body force field is chosen for the nonbonded interactions and its parameters are fitted by demanding that the radial distribution function (rdf) obtained from a small detailed sample match that from a coarse grained one [22,23]. Standard op-

timization techniques are used to converge on the detailed rdf by iteratively adjusting the parameters in the nonbonded force field.

A somewhat different procedure [32–34] that has been used for coarse-graining biomolecules involves demanding that all other simulation conditions remaining same, the net force on the group of atoms constituting a superatom in the united atom representation should equal the force on the superatom itself in the CG representation. Note that the force on the superatom in the CG system comes from bonded as well as nonbonded interactions. Izvekov *et al.* [32,34] have demonstrated that for certain biomolecules, this “force matching” technique yields a close match to the rdf between the detailed and CG systems. We adopt this technique as a starting point for our coarse graining scheme. Unlike in Mulder *et al.* [26–28], we perform a 1:1 coarse graining, i.e., each monomer of PS is represented by one superatom in the coarse-grained system. Moreover, our method puts bonded and nonbonded parameters on equal footing and though we do not target to match the rdf exactly, a reasonable match is obtained. Also, following the CG procedure a pressure match is performed.

This paper is organized in the following manner. In the next section we briefly describe the united atom force field for PS that we have adopted from Mondello *et al.* [13]. A sample of PS prepared and equilibrated with this united atom force field will be called a “detailed sample” in this paper. The algorithm for the force matching technique that we have used for calibrating both bonded and nonbonded force fields is presented in Sec. III. In the Sec. IV we present the calibrated parameters for coarse-grained polystyrene and show that the quality of coarse-graining is equivalent to other techniques. We turn to the simulation of the stress-strain response of polystyrene in Sec. V and discuss additional modifications to the CG scheme that is required for obtaining a set of CG parameters that reproduce the stress-strain response satisfactorily. Salient conclusions from this work are presented in Sec. VI.

In this work we will use lower case Roman and Greek alphabets to denote quantities pertaining to the detailed united atom system and upper case ones for the coarse grained system.

## II. DETAILED FORCE FIELDS FOR POLYSTYRENE

The detailed force field for polystyrene is adopted from Mondello *et al.* [13] and is briefly described here. The numbering refers to Fig. 2 which shows two consecutive polystyrene monomers. As mentioned earlier, in this united atom representation, the hydrogen atoms are not explicitly accounted for and are clubbed into the bonded carbon. In Fig. 2, the atoms numbered 1–6 (also 9–14 in the second monomer) are aromatic carbons while 7 and 8 (also 15 and 16 in the second monomer) are aliphatic. Bond lengths are maintained constant at

1.53 Å between two aliphatic carbons (e.g., between atoms 8–7 or 7–16),

1.51 Å between an aliphatic and an aromatic carbon (e.g., between atoms 7 and 1),

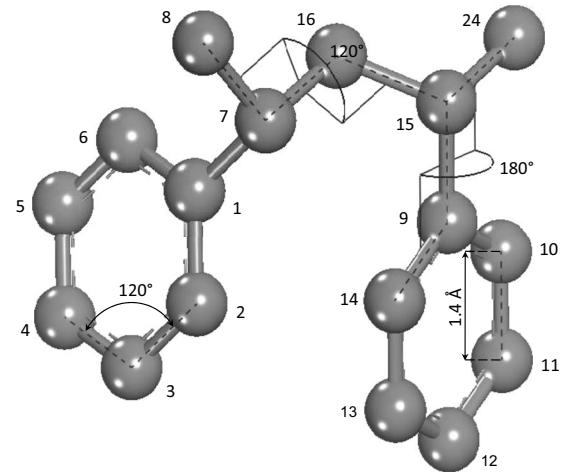


FIG. 2. United atom model of PS with labeled atoms to facilitate description of the detailed force field.

1.40 Å between two aromatic carbons (e.g., between atoms 14 and 13),  
using the SHAKE algorithm [35] with a tolerance of 0.0004 Å.

The bond angle potential for a generic bond angle  $\theta$  in the united atom model is of the form

$$v_{\theta} = k_{\theta}(\theta - \theta_0)^2, \quad (6)$$

where  $\theta_0$  is the equilibrium value of the bond angle and  $k_{\theta}$  is the stiffness. The values of  $k_{\theta}$  and  $\theta_0$  are defined as follows

$k_{\theta}, \theta_0 = 60 \text{ kcal/mol}, 109.5^{\circ}$  for aliphatic  $\text{CH}_2\text{-CH-CH}_2$ ,

(e.g., between atoms 8–7–16),

63 kcal/mol,  $109.5^{\circ}$  for aliphatic  $\text{CH-CH}_2\text{-CH}$ ,

(e.g., between atoms 7–16–15),

60 kcal/mol,  $109.5^{\circ}$  for  $\text{CH}_2(\text{aliph})\text{-CH}(\text{aliph})\text{-C}(\text{arom})$ ,

(e.g., between atoms 8–7–1), and

70 kcal/mol,  $120.0^{\circ}$  for  $\text{CH}(\text{aliph})\text{-C}(\text{arom})\text{-CH}(\text{arom})$ ,

(e.g., between atoms 7–1–6).

Similarly, the torsion angle potential for a generic dihedral angle  $\phi$  is of the form

$$v_{\phi} = k_{\phi}(1 - \cos 3\phi), \quad (7)$$

governing rotation of a dangling phenyl ring around the main chain i.e., for torsion between  $\text{X-CH aliphatic-CH}_2 \text{ aliphatic-X}$  (e.g., between atoms 8–7–16–15). The stiffness  $k_{\phi} = 1.4 \text{ kcal/mol}$  and a minima of the potential occurs at  $120^{\circ}$ . On the other hand, the torsion potential governing rotation of a phenyl ring about an axis passing through say, 15–9–12 (i.e., about a  $\text{CH aliphatic -C aromatic bond}$ , e.g., between atoms 24–15–9–14) is given by

$$v_\phi = k_\phi \cos^2(\phi - \phi_0), \quad (8)$$

where,  $k_\phi = 2$  kcal/mol and  $\phi_0 = 90^\circ$ .

Nonbonded interactions are modeled using Lenard Jones potentials of the form

$$v_{nb} = \epsilon [(\rho/r)^{12} - 2(\rho/r)^6]. \quad (9)$$

The parameters in the LJ potential are defined for the different interactions as

$\epsilon, \rho = 0.12$  kcal/mol,  $4.321$  Å for aliphatic  $\text{CH}_2$ ,

$= 0.09$  kcal/mol,  $4.153$  Å for aliphatic CH, and,

$= 0.12$  kcal/mol,  $4.153$  Å for aromatic C and CH.

Interactions between different species of nonbonded atoms are handled using the geometric mean of the individual  $\epsilon$  values and arithmetic mean of the  $\rho$  values.

A few modifications to the original model have been made here. First, the tetrahedral arrangement between atoms say, 7–16–8–1 or 15–24–16–9 has been maintained by assigning a harmonic improper dihedral potential of the form

$$v_\phi = \frac{1}{2} k'_\phi (\phi - \phi_0)^2, \quad (10)$$

with  $k'_\phi = 100$  kcal/mol and  $\phi_0 = 36^\circ$ . Second, each phenyl ring is kept confined to its plane by the use of rigid pseudo-bonds between its vertices (e.g., between atoms 1–4, 2–5, and 3–6). Periodic boundary conditions (pbc) are used in all simulations reported in this work.

Using the force field described above, a detailed sample containing 14 PS chains with 80 monomers per chain was first equilibrated at 500 K. The equilibration was performed at a pressure of 0.1 MPa, at which the sample attained a density of  $0.8$  g/cm<sup>3</sup>, close to the experimentally observed density of PS. In order to obtain a glassy sample, the united atom sample at 500 K was quenched under constant pressure, at a moderate rate of 1 K/Ps, to 100 K. The variation of the specific volume of the sample  $v_f$  with temperature  $T$  is shown in Fig. 3(a). Straight lines fitted to the high and low temperature data intersect at  $T_g \approx 355$  K indicating that at 100 K, where we perform the subsequent uniaxial deformations, the sample is well in the glassy regime. The exact value of  $T_g$  obtained from MD simulations depends largely on the cooling rate  $\dot{T}$  and pressure and weakly on the thermostat and barostat constants used. It is also somewhat affected by the process of fitting two straight lines to the high and low-temperature data and the determination of  $T_g$  from their intersection. Thus, a large variation is expected in  $T_g$  values obtained by different authors. In fact, Lyulin *et al.* [7] report a value of 385 K at a  $\dot{T} = 0.05$  K/ps, obtained using different thermostat and barostat constants. Faller [36] reports a value of about 320 K while Santangelo and Roland [37] show that the value of  $T_g$  depends strongly on the molecular weight till a chain length of about 200 monomers/

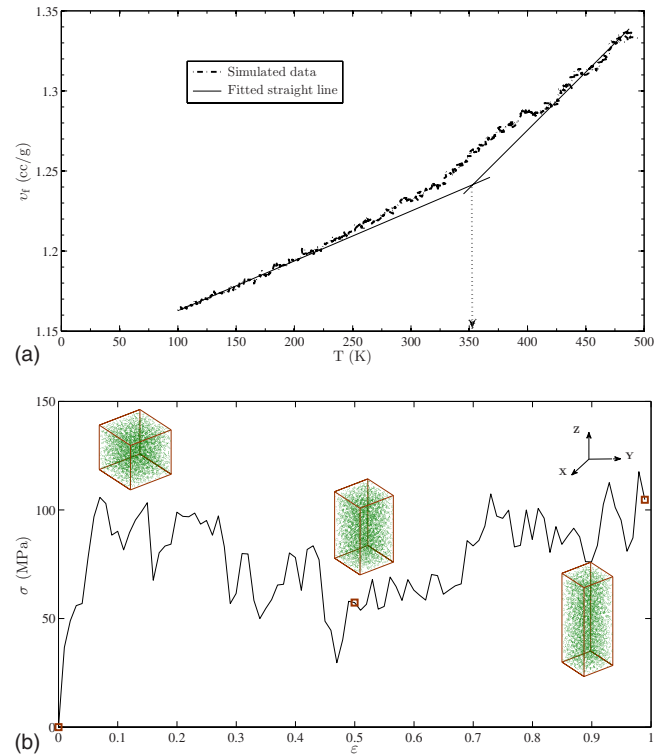


FIG. 3. (Color online) (a) Variation in the specific volume  $v_f$  with temperature for the united atom PS sample cooled from 500 to 100 K at  $\dot{T} = 1$  K/ps. (b) Stress-strain response of the detailed sample at 100 K pulled in incompressible tension at a rate of  $0.005$  ps<sup>-1</sup>. Deformed configurations at the strain marked by square symbols are superposed.

chain. We chose a glassy temperature of 100 K in order to be sure that we are well below the glass transition temperature even after taking all the uncertainties in the determination of  $T_g$  into consideration.

The variation in the  $z$ - $z$  component of the virial stress  $\sigma$  with the overall imposed engineering strain  $\epsilon$  for the same sample at 100 K is shown in Fig. 3(b). The sample is deformed in an incompressible manner by increasing one of the cell vectors at a constant rate of  $0.296$  Å/ps which corresponds to an engineering strain rate  $\dot{\epsilon}$  of approximately  $0.005$  ps<sup>-1</sup>. Along the other two directions (i.e.,  $x$  and  $y$ ), equal compressive strains are applied at a rate that keeps the volume of the entire simulation box constant. The stress-strain response exhibits an initial elastic part, a drop following yield at about 105 MPa, and finally a moderate hardening response at high strains. The Young's modulus, measured from the stress-strain curve is about 3.6 GPa. This is comparable to the value of 2.9 GPa obtained by Lyulin *et al.* [7] at  $\dot{\epsilon} \approx 10^{-4}$  ps<sup>-1</sup>. The behavior is qualitatively similar to what is experimentally observed for PS. This stress-strain response obtained from the detailed sample will be the benchmark that CG simulations will have to follow. Undeformed and deformed configurations of the simulation box for the detailed force field are also shown at the marked points on the stress-strain curve.

### III. COARSE-GRAINING PROCEDURE: THE FORCE MATCHING TECHNIQUE

A superatom  $I$  in our case is one whole monomer of PS. The superatom is placed at  $\mathbf{R}_I$ , the mass center of the monomer, i.e.,

$$\mathbf{R}_I = \sum_{i=1}^p m_i \mathbf{r}_i / \sum_{i=1}^p m_i, \quad (11)$$

where  $p$  is the number of united atoms in a monomer.

We want the force on superatom  $I$  to be the vector sum of the forces  $\mathbf{f}_i$  acting on the  $p$  united atoms constituting it, i.e.,

$$\mathbf{F}_I^{ref} = \sum_{i=1}^p \mathbf{f}_i. \quad (12)$$

As in Izvekov *et al.* [32], we define an objective function,

$$\Pi = \frac{1}{3LN} \sum_{L=1}^M \sum_{I=1}^N |\mathbf{F}_{I,L}^{ref} - \mathbf{F}_{I,L}|^2, \quad (13)$$

where  $N$  is the total number of superatoms in the system and  $(\cdot)_{I,L}$  denotes a physical quantity on superatom  $I$  in the  $L$ -th configuration. The function  $\Pi$  involves an average over all the superatoms in all the configurations on which the force matching is to be done. With the understanding that  $\Pi$  is constructed as an average over many configurations of the same system (e.g., a number of snapshots taken along a  $NVT$  run), we will drop the subscript  $L$  in subsequent equations. The objective then is to find  $\mathbf{F}_I$  such that  $\Pi$  is a minimum.

The force  $\mathbf{F}_I$  acting on superatom  $I$  is assumed to result from inter and intrachain central pairwise nonbonded forces as well as harmonic bond stretching and bending forces with intrachain neighbors. The nonbonded force on superatom  $I$  is of the form

$$\mathbf{F}_I^{nb} = \sum_{K=1}^{N_{nb}} F(R_{IK}) \hat{\mathbf{R}}_{IK}, \quad (14)$$

where, the summation is taken over the  $N_{nb}$ , nonbonded neighbors of atom  $I$ . The distance vector is given as  $\mathbf{R}_{IK} = \mathbf{R}_I - \mathbf{R}_K$ , while the unit vector along it is denoted by  $\hat{\mathbf{R}}_{IK} = \mathbf{R}_{IK}/R_{IK}$ , where for any vector  $\mathbf{R}_{IJ} = |\mathbf{R}_{IJ}|$ .

Along with the nonbonded CG force field, we also determine the bonded CG force fields through the force matching technique. Thus, the bonded forces also contribute to the force  $\mathbf{F}_I$ . Bond stretching force on atom  $I$  due to an atom  $J$  bonded to it is given by the equation,

$$\mathbf{F}_{IJ} = -\frac{1}{R_{IJ}} \left[ \frac{\partial}{\partial R_{IJ}} \mathcal{U}_s(R_{IJ}) \right] \mathbf{R}_{IJ}, \quad (15)$$

where the bond stretching potential  $\mathcal{U}_s(R_{IJ})$  between two superatoms  $I$  and  $J$  is taken to be harmonic of the form:

$$\mathcal{U}_s(R_{IJ}) = \frac{1}{2} K_s (R_{IJ} - R_0)^2. \quad (16)$$

The equilibrium bond distance  $R_0$  and the stiffness  $K_s$  are yet undetermined.

Using the labeling of atoms used in Fig. 1(b), the net bond stretching force  $\mathbf{F}_I^s$  on superatom  $I$  is the vector summation of the forces due to neighboring superatoms  $J$  and  $K$  and is given as:

$$\mathbf{F}_I^s = -K_s (R_{IJ} - R_0) \hat{\mathbf{R}}_{IJ} - K_s (R_{IK} - R_0) \hat{\mathbf{R}}_{IK}. \quad (17)$$

An alternate way of writing the above equation that will be useful later is as follows:

$$\begin{aligned} \mathbf{F}_I^s &= [(-R_{IJ} \hat{\mathbf{R}}_{IJ} - R_{IK} \hat{\mathbf{R}}_{IK}) \quad (\hat{\mathbf{R}}_{IJ} + \hat{\mathbf{R}}_{IK})] \begin{Bmatrix} K_s \\ K_s R_0 \end{Bmatrix} \\ &= \mathbf{S}_I \begin{Bmatrix} K_s \\ K_s R_0 \end{Bmatrix}. \end{aligned} \quad (18)$$

In the above,  $\mathbf{S}_I$  is a  $3 \times 2$  matrix embodying the contribution due to bond stretching forces for  $I^{\text{th}}$  superatom using  $K_s$  and  $K_s R_0$  as the parameters to be determined while minimizing  $\Pi$ .

A similar procedure may be adopted to determine the force due to bond bending on superatom  $I$  and  $\mathbf{F}_I^b$ . To this end, we again assume a harmonic bond bending potential for a generic bond angle  $\Theta_{JK}$  [see, Fig. 1(b)]

$$\mathcal{U}_b(\Theta_{JK}, R_{IJ}, R_{IK}) = \frac{1}{2} K_\Theta (\Theta_{JK} - \Theta_0)^2, \quad (19)$$

where, as for the bond stretching,  $K_\Theta$  and the equilibrium bond angle  $\Theta_0$  are yet undetermined parameters. The force on superatom  $I$  due to changes in the bond angle  $\Theta_{JK}$  is given by:

$$\mathbf{F}_I^b = -\frac{\partial}{\partial \mathbf{R}_I} \mathcal{U}_b(\Theta_{JK}, R_{IJ}, R_{IK}). \quad (20)$$

As shown in Fig. 1(b), the force on superatom  $I$  due to bond bending is due to the bond angles  $\Theta_{LJ}$ ,  $\Theta_{JK}$ , and  $\Theta_{IKM}$ . Thus, the force  $\mathbf{F}_I^b$  can be written as,

$$\begin{aligned} \mathbf{F}_I^b &= [C_1 \Theta_{LJ} \hat{\mathbf{R}}_1 + C_2 \Theta_{JK} \hat{\mathbf{R}}_2 + C_3 \Theta_{IKM} \hat{\mathbf{R}}_3 \\ &\quad - C_1 \hat{\mathbf{R}}_1 - C_2 \hat{\mathbf{R}}_2 - C_3 \hat{\mathbf{R}}_3] \begin{Bmatrix} K_\Theta \\ K_\Theta \Theta_0 \end{Bmatrix} = \mathbf{B}_I \begin{Bmatrix} K_\Theta \\ K_\Theta \Theta_0 \end{Bmatrix}, \end{aligned} \quad (21)$$

where, such as  $\mathbf{S}_I$  and  $\mathbf{B}_I$  is a  $3 \times 2$  matrix embodying the contribution to the force on superatom  $I$  due to bond bending,  $C_1$ ,  $C_2$ , and  $C_3$  are constants and the minimization process of  $\Pi$  is expected to yield values of  $K_\Theta$  and  $K_\Theta \Theta_0$ .

Finally, the method due to Izvekov *et al.* [32] is closely followed to parametrize the nonbonded potential. As described in Eq. (14), the key ingredient in the nonbonded force field is the function  $F(R)$ . At this stage, we do not assume a functional form for  $F(R)$ . The range of  $R$  ( $R_{\min} \leq R \leq R_c$ , where  $R_c$  is the cut-off distance for the nonbonded forces) is divided into a large number of points,  $P$ , spaced  $\Delta R$  apart. In the  $k^{\text{th}}$  interval where,  $R_k < R < R_{k+1}$ , the function  $F(R)$  is approximated by a piecewise cubic polynomial function as,

$$F(R) = A_k + B_k R + C_k R^2 + D_k R^3, \quad R_k < R < R_{k+1}, \quad (22)$$

where,  $A_k$ ,  $B_k$ ,  $C_k$ , and  $D_k$  denote coefficients of the polynomial. The function  $F(R)$  can be reparametrized in terms of its functional values  $F_k$ ,  $F_{k+1}$  and the second derivatives,  $F''_k$  and  $F''_{k+1}$  at the  $k^{\text{th}}$  and  $(k+1)^{\text{th}}$  points. It can be shown that the reparametrized form of  $F(R)$  is given by,

$$F(R) = a_k(R, R_1, \dots, R_P)F_k + b_k(R, R_1, \dots, R_P)F_{k+1} + c_k(R, R_1, \dots, R_P)F''_k + d_k(R, R_1, \dots, R_P)F''_{k+1}, \quad (23)$$

$$R_k < R < R_{k+1},$$

where,

$$a_k = \frac{(R_{k+1} - R)}{(R_{k+1} - R_k)},$$

$$b_k = \frac{(R - R_k)}{(R_{k+1} - R_k)},$$

$$c_k = \frac{(2R_k R_{k+1}^2 - R_k^2 R_{k+1})}{6(R_{k+1} - R_k)} + \frac{(R_k^2 - 2R_k R_{k+1} - 2R_{k+1}^2)}{6(R_{k+1} - R_k)} R + \frac{R_{k+1}}{2(R_{k+1} - R_k)} R^2 - \frac{1}{6(R_{k+1} - R_k)} R^3,$$

$$d_k = \frac{(R_k R_{k+1}^2 - 2R_{k+1} R_k^2)}{6(R_{k+1} - R_k)} + \frac{(2R_k^2 + 2R_k R_{k+1} - R_{k+1}^2)}{6(R_{k+1} - R_k)} R - \frac{R_k}{2(R_{k+1} - R_k)} R^2 + \frac{1}{6(R_{k+1} - R_k)} R^3.$$

Thus, for  $R_k < R < R_{k+1}$  we can write

$$F(R) = \begin{bmatrix} 0 & 0 & \dots & a_k & c_k & b_k & d_k & \dots & 0 & 0 \end{bmatrix} \begin{Bmatrix} F_1 \\ F''_1 \\ F_2 \\ F''_2 \\ \vdots \\ F_k \\ F''_k \\ F_{k+1} \\ F''_{k+1} \\ \vdots \\ F_{P-1} \\ F''_{P-1} \\ F_P \\ F''_P \end{Bmatrix} = \mathbf{A}_k \mathbf{D}. \quad (24)$$

Here on the right hand side  $\mathbf{A}_k$  is a  $1 \times (2P+2)$  matrix for the  $k^{\text{th}}$  interval and  $\mathbf{D}$  is a vector containing the nodal values of  $F(R)$  and their second derivatives. Thus, if two nonbonded superatoms  $I$  and  $J$  are separated by a distance,  $R_{IJ}$ , where

$R_k < R_{IJ} < R_{k+1}$ , the force on superatom  $I$  due to  $J$  following Eq. (14), is

$$\mathbf{F}_{IJ} = \mathbf{A}_k \mathbf{D} \frac{R_{IJ}}{R_{IJ}}, \quad (25)$$

where,  $\mathbf{A}_k(R_{IJ}/R_{IJ})$  is a  $3 \times (2P+2)$  system.

Finally, after performing this procedure for all superatoms of a configuration and minimizing the objective function in Eq. (13) we get,

$$[\mathbf{A} \quad \mathbf{S} \quad \mathbf{B}] \begin{Bmatrix} \mathbf{D} \\ K_s \\ K_b \\ K_s R_0 \\ K_b \Theta_0 \end{Bmatrix} = \{\mathbf{F}^{ref}\} = [\mathbf{K}]\{X\}, \quad (26)$$

where the finally assembled matrix  $\mathbf{K}$  is a  $3N \times (2P+6)$  matrix,  $X$  and  $\mathbf{F}^{ref}$  are  $(2P+6) \times 1$  and  $3N \times 1$  vectors, respectively. The matrix  $\mathbf{K}$  is rectangular and so the system can only be solved in a least square sense. For our purpose, we use, singular value decomposition of  $\mathbf{K}$  to obtain its pseudo-inverse, which when multiplied with  $\mathbf{F}^{ref}$  gives the least square solution  $X$ . After the solution is obtained, the equilibrium values of bond length and bond angle,  $R_0$  and  $\Theta_0$  as well as the variation of  $F(R)$  with  $R$  is easily obtained. The process is repeated over many configurations and the final coarse grained potentials are obtained by averaging the parameters over all the configurations used.

The efficacy of the method outlined depends on a number of factors. The force matching method entails the pseudo inversion of  $\mathbf{K}$ , which is a  $3N \times (2P+6)$  matrix where in general  $3N \geq (2P+6)$ . We have observed that a large value of  $P$  is needed to obtain a piecewise low order polynomial approximation to  $F(R)$  (we have used a cubic polynomial and using an even lower order polynomial will need a much larger  $P$ ). The appropriate value of  $P$  also depends on the number of zero crossings of  $F(R)$  and as a result will need to be chosen carefully in each case. In our case, we chose  $P = 50$  which gives a satisfactory nonbonded CG potential for PS.

#### IV. FORCE MATCHING TECHNIQUE FOR PS

Figure 4(a) shows the function  $F(R)$  derived from the force matching technique for PS. The function is truncated for  $R < 5 \text{ \AA}$  since there were too few or no superatoms separated by less than  $5 \text{ \AA}$ . The force between two superatoms become almost zero beyond  $10 \text{ \AA}$ , which then is a natural cut-off distance for the CG system. Figure 4(b) shows the nonbonded potential  $\mathcal{U}(R)$  obtained by integrating the force field. Nonbonded separations below  $5 \text{ \AA}$  are inaccessible to superatoms and therefore we have added a steep wall on the potential at  $5 \text{ \AA}$ . The potential has a pronounced minima at around  $7.5 \text{ \AA}$ .

Parameters for the bond stretching and bending potentials are also obtained from the minimization procedure. For the specific case of united atom PS, the obtained values are  $K_s = 4.5 \text{ kcal/mol-\AA}^2$  and  $K_b = 8.827 \text{ kcal/mol}$  while  $R_0 = 5 \text{ \AA}$  and  $\Theta_0 = 122.7^\circ$ .

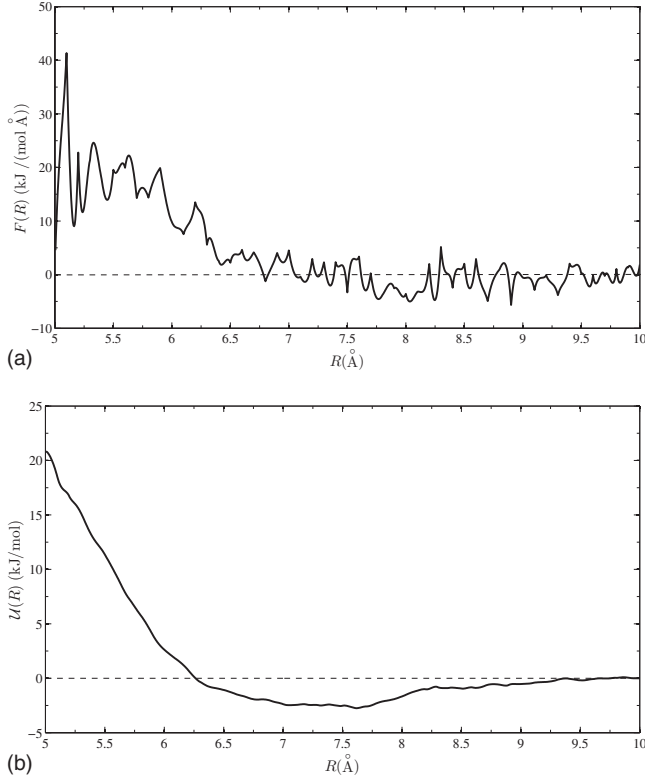


FIG. 4. The (a) nonbonded force and (b) potential  $\mathcal{U}(R)$  for the equivalent CG polystyrene obtained by the force matching technique.

Using the CG force field obtained from the force matching technique, we have equilibrated a CG ensemble at 500 K that was obtained from the united atom PS described earlier. The CG sample at the onset of the equilibration process is constructed on the same detailed PS sample (at 500 K) as described in the last section, with the superatoms being placed at the mass centers of each monomer of the united atom model. Thus the CG system also consists of 14 CG chains with 80 superatoms, each having a mass of 104 amu.

To assess whether the CG bonded force field parameters are reasonable, we also used an alternate technique to obtain them. Here, we again used the same detailed sample described in the previous section and extracted the probability distributions  $P'_s(R)$  and  $P'_b(\Theta)$  of the CG bond lengths and angles, respectively. The scaled probabilities  $P_s(R)$  and  $P_b(\Theta)$  for the bond lengths and angles, respectively, are obtained from the probability distributions  $P'_s(R)$  and  $P'_b(\Theta)$  as

$$P_s(R) \propto \frac{P'_s(R)}{R^2},$$

$$P_b(\Theta) \propto \frac{P'_b(\Theta)}{\sin \Theta}.$$

Further assuming that the CG bonded potential factorizes, i.e.,

$$\mathcal{U}(R, \Theta) = \mathcal{U}_s(R)\mathcal{U}_b(\Theta), \quad (27)$$

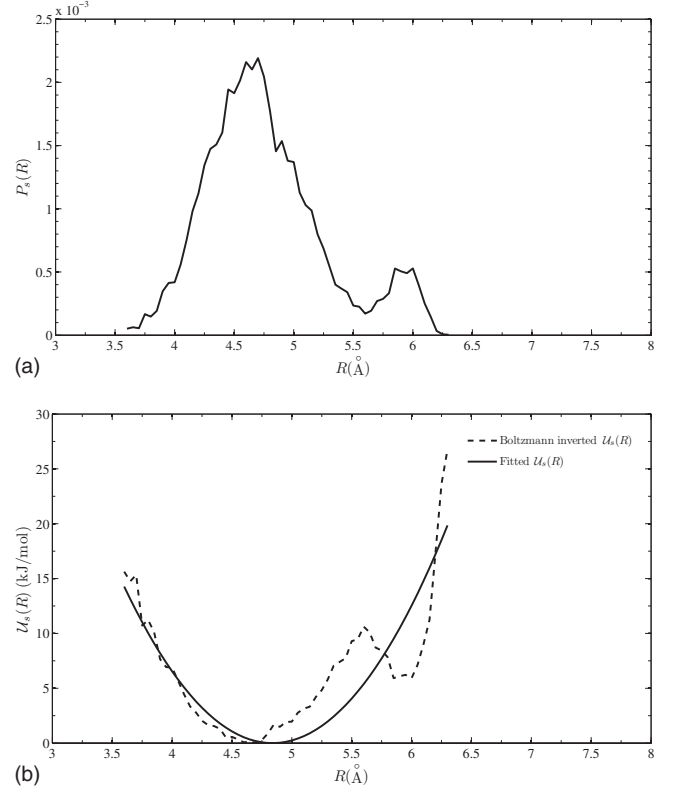


FIG. 5. The (a) normalized probability distribution  $P_s(R)$  of CG bond lengths and (b) the corresponding Boltzmann inverted potential  $\mathcal{U}_s(R)$  for CG bond stretching. Also shown is the fit using the harmonic potential.

allows us to write the coarse grained potentials by Boltzmann inversion as

$$\mathcal{U}_s(R) = -k_B T \ln P_s(R),$$

$$\mathcal{U}_b(\Theta) = -k_B T \ln P_b(\Theta).$$

where  $k_B$  is the Boltzmann constant. For example, the probability and potential for bond stretching obtained by this method are shown in Figs. 5(a) and 5(b) along with the fits to the inverted potentials using Eq. (16). The minima of the bond stretching potential lies at 4.65 Å compared to 5 Å for the force matched case. For the bond bending potential too, the equilibrium bond angle turns out to be 120° compared to 122.7° obtained by the force matching method.

Further, we compared the nonbonded part of the rdf  $g_{nb}$  obtained from the detailed united atom simulation with that obtained from the CG sample equilibrated using the force field from the force matching technique. Note that many coarse-graining schemes use the nonbonded part of the rdf obtained from the detailed sample as the starting point for optimizing the parameters of the nonbonded force field [23]. In our case, as shown in Fig. 6, even though our method exercises no control on the rdf, the nonbonded rdf for the detailed sample is matched remarkably well by the CG sample.

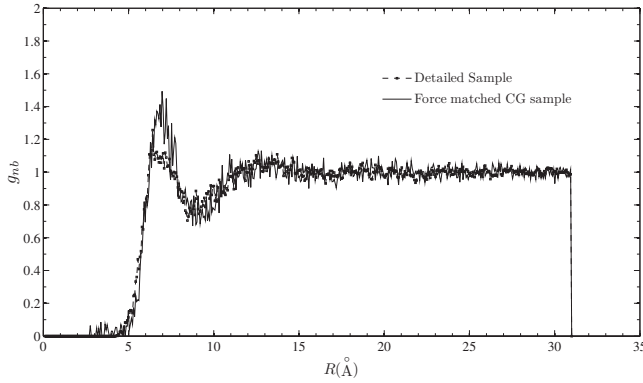


FIG. 6. Comparison between the nonbonded rdfs of the detailed and CG samples of PS containing 14 chains of 80 monomer each.

### V. STRESS-STRAIN RESPONSE OF CG SAMPLES

It is in place here to reiterate the aim of this work. We intend to formulate a CG force field for PS that reproduces the stress-strain response of a detailed united atom sample of the same material. The coarse-graining, it should be noted, is done at a higher temperature. Both the coarse-grained and the detailed samples are then quenched to below  $T_g$  and imparted the requisite deformation.

Even at higher temperatures, after the CG force field has been obtained, a major problem remains. The CG sample, at 500 K, does not have the same level of pressure (volume) as the detailed sample when held in a  $NVT$  ( $NPT$ ) ensemble. In fact, to be held at the same volume and temperature, the CG sample requires an almost 15 times larger pressure compared to its detailed counterpart. The atomic virial, that enters the evaluation of the pressure, in the CG sample, is much lower compared to the detailed sample since the intramonomeric contribution to the virial is completely lost during the coarse graining procedure. Obviously, a match in the stresses cannot be expected with such a huge mismatch in the pressure.

At this point, we choose to further iteratively refine the nonbonded force field at 500 K with a view to equalizing the pressure in the CG and detailed samples. The strategy follows assuming a parametric form of the nonbonded force field (much in the spirit of Sun and Faller [23] and Muller-Plathe [22]) whose parameters are to be obtained so as to minimize the squared difference  $\Delta p$  between the block averaged pressures obtained from the detailed and CG samples in a long  $NVT$  run at 500 K. Thus we minimize

$$\chi^2 = \sum_{i=1}^{N_{block}} \Delta p_i^2, \quad (28)$$

where  $N_{block}$  is the number of blocks into which the data is divided using a block size of 20 time data points. The initial guess for the parameters comes from the nonbonded force field that we have obtained from the force matching technique.

To start with, we assume that the nonbonded force field has the form of an LJ potential, i.e.,

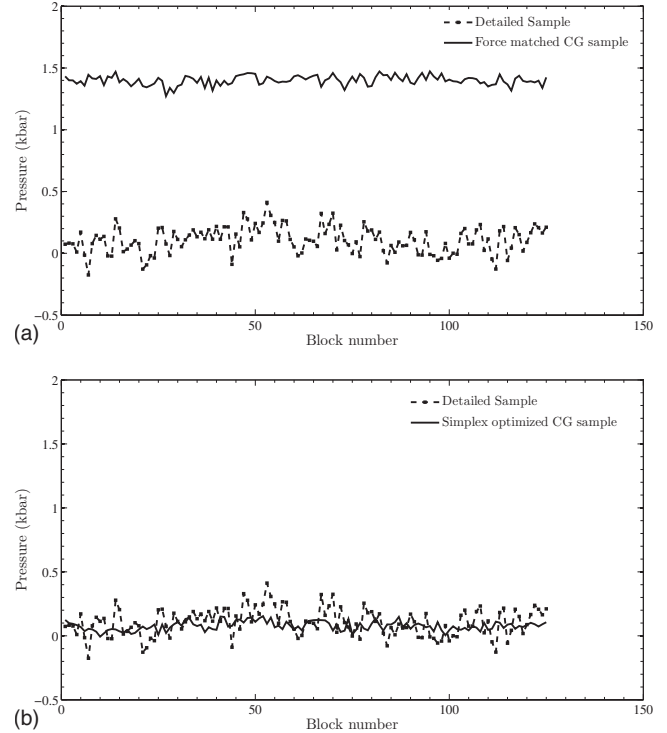


FIG. 7. Comparison of block averaged pressure variation at 500 K under  $NVT$  control for a detailed and a CG sample, (a) before and (b) after simplex optimization.

$$U_{nb}(R) = 4U_0 \left[ \left( \frac{\varrho_0}{R} \right)^{12} - \left( \frac{\varrho_0}{R} \right)^6 \right],$$

which, when fitted to the force field in Fig. 4(b), yields the initial guess parameters  $\varrho_0 = 6.4 \text{ \AA}$  and  $U_0 = 0.081 \text{ kcal/mol}$ . Following Faller and co-workers [38] we use the Nelder-Mead simplex algorithm [39] to optimize  $U_0$  and  $\varrho_0$  till the CG and the detailed samples require the same level of pressure to be held in a  $NVT$  ensemble at a given temperature and volume. A simplex scheme is useful in this case as it requires, for the minimization of  $\chi^2$ , only evaluations of the functional values and not its derivatives. Figure 7(a) and 7(b) shows the variation in pressure in a CG and a detailed sample held at the same volume and 500 K at the end of the force matching process and after the simplex algorithm has converged. The final nonbonded force field parameters are  $\varrho_0 = 6.4 \text{ \AA}$  and  $U_0 = 1.609 \text{ kcal/mol}$  indicating that the simplex optimization leaves the  $\varrho_0$  unchanged. This is also reflected in Fig. 8 where we compare the nonbonded parts of the rdf between the detailed and the simplex optimized sample. The location of the peak in the rdf is retained at  $R = \varrho_0$ . However, the height of the first peak is enhanced due to the pressure correction. Note that matching the rdf does not guarantee closeness of pressure or stress between the detailed and CG samples.

At this juncture, we have a detailed and a CG sample at 500 K that have similar rdfs and closely matched pressure. The CG sample is now quenched at a rate of 1 K/ps, undergoes glass transition at  $T_g \approx 268 \text{ K}$  and is deformed in the same manner as the detailed sample (see Sec. II) at 100 K.

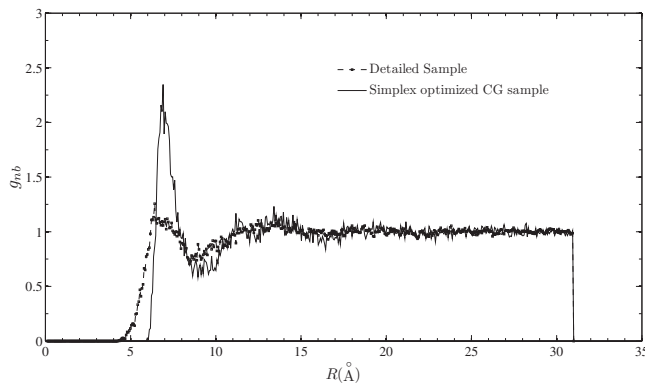


FIG. 8. Comparison of rdfs between the detailed and the simplex optimized CG samples.

The stress-strain responses of the detailed and the quenched CG samples are shown in Fig. 9. Note that after quenching, there is no guarantee that the densities of the CG and detailed samples are identical and our simulations with PS show that there is indeed a slight difference. Both the CG and the detailed systems contain 14 chains with 80 monomers/chain, respectively. Thus the CG system has eight times less atoms than the detailed sample. But, the stress-strain curve obtained for the CG sample is very close to that obtained by the detailed sample.

The noise in the stress-strain curve is typical of small samples. We also generated a larger CG sample with 200 chains of 80 monomers/chain and used the derived force field to equilibrate it at high temperature. The stress-strain curve obtained for this sample, also shown in Fig. 9, still follows that of the detailed sample closely but is devoid of the noise.

## VI. CONCLUSIONS

Molecular dynamics simulations of stress-strain response of amorphous polymers are conducted at temperatures well below their glass transition. Using detailed models of these materials, given the present computational resources, severely restricts the length and time scales of samples that can be simulated. We have outlined a systematic coarse-graining procedure where we start with identifying each monomer of

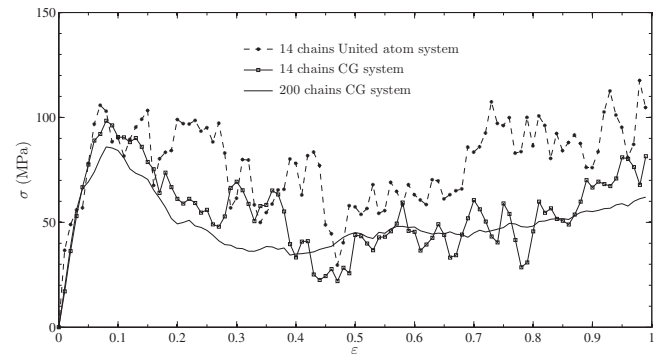


FIG. 9. Comparison between the stress-strain response of detailed and two CG polystyrene samples deformed at a rate of  $0.005 \text{ ps}^{-1}$  at 100 K.

polystyrene with one CG superatom, thus effecting a eight-fold decrease in computational requirement.

The force matching technique is adopted for coarse-graining detailed PS at a high temperature. We have demonstrated that bonded potentials obtained through this technique are comparable to those obtained by other methods. The nonbonded force field is also estimated well, which is proved by the fact that the coarse grained, nonbonded part of the rdf approximates the one of the detailed sample to a high degree of accuracy. However, like any coarse graining scheme, the pressure in the CG system is not equal to the detailed system under same conditions of temperature and volume.

We therefore propose to iteratively refine the nonbonded potential further with a view to equalizing the pressure under similar conditions of volume and temperature. To do this, the nonbonded force field from the force matching technique is used as a starting point for the iterative refinement, which follows a simplex algorithm. In fact, assuming a two parameter nonbonded force field (akin to the LJ potential), we are able to accomplish the pressure equalization quite easily and effectively. Thus a complete coarse graining of PS is accomplished at a high temperature much above  $T_g$ . All PS samples thus coarse grained, when quenched and subsequently deformed at the same rates below  $T_g$ , are shown to yield very similar stress-strain curves, which, in turn, approximates the stress-strain response of the detailed PS sample quite well.

- 
- [1] D. N. Theodorou, *Mol. Phys.* **102**, 147 (2004).  
 [2] D. Brown and J. H. R. Clarke, *Macromolecules* **24**, 2075 (1991).  
 [3] I. Ogura and T. Yamamoto, *Polymer* **36**, 1375 (1995).  
 [4] F. M. Capaldi, M. C. Boyce, and G. C. Rutledge, *Phys. Rev. Lett.* **89**, 175505 (2002).  
 [5] K. Yashiro, T. Ito, and Y. Tomita, *Int. J. Mech. Sci.* **45**, 1863 (2003).  
 [6] A. Negi and S. Basu, *Model. Simul. Mater. Sci. Eng.* **14**, 563 (2006).  
 [7] A. V. Lyulin, B. Vorselaars, M. A. Mazo, N. K. Balabaev, and M. A. J. Michels, *Europhys. Lett.* **71**, 618 (2005).  
 [8] J. H. Weiner and J. Gao, *Model. Simul. Mater. Sci. Eng.* **2**, 755 (1994).  
 [9] M. J. Stevens, *Macromolecules* **34**, 2710 (2001).  
 [10] J. Rottler and M. O. Robbins, *J. Adhes. Sci. Technol.* **17**, 369 (2003).  
 [11] U. Kulmi and S. Basu, *Model. Simul. Mater. Sci. Eng.* **14**, 1071 (2006).  
 [12] D. Steele, *J. Chem. Soc., Faraday Trans. 2* **81**, 1077 (1985).  
 [13] M. Mondello, H. J. Yang, H. Furuya, and R. J. Roe, *Macromolecules* **27**, 3566 (1994).

- [14] D. K. Mahajan and S. Basu, *Int. J. Appl. Mech.* (to be published).
- [15] M. Fukuda and S. Kuwajima, *J. Chem. Phys.* **107**, 2149 (1997).
- [16] R. S. Hoy and M. O. Robbins *J. Polym. Sci., Part B: Polym. Lett.* **44**, 3487 (2006).
- [17] M. Bulacu and E. van der Giessen, *J. Chem. Phys.* **123**, 114901 (2005).
- [18] M. Kröger, *Phys. Rep.* **390**, 453 (2004).
- [19] W. Tschöp, K. Kremer, J. Batoulis, T. Bürger, and O. Hahn, *Acta Polym.* **49**, 61 (1998).
- [20] R. L. C. Akkermans and W. J. Briels, *J. Chem. Phys.* **114**, 1020 (2001).
- [21] J. Baschnagel *et al.*, *Adv. Polym. Sci.* **152**, 41 (2000).
- [22] F. Muller-Plathe, *ChemPhysChem* **3**, 754 (2002).
- [23] Q. Sun and R. Faller, *Comput. Chem. Eng.* **29**, 2380 (2005).
- [24] H. G. H. van Melick, L. E. Govaert, and H. E. H. Meijer, *Polymer* **44**, 2493 (2003).
- [25] J. Lai and E. van der Giessen, *Mech. Mater.* **25**, 183 (1997).
- [26] T. Mulder, V. A. Harmandaris, A. V. Lyulin, N. F. A. van der Vegt, K. Kremer, and M. A. J. Michels, *Macromolecules* **42**, 384 (2009).
- [27] T. Mulder, V. A. Harmandaris, A. V. Lyulin, N. F. A. van der Vegt, and M. A. J. Michels, *Macromol. Theory Simul.* **17**, 393 (2008).
- [28] T. Mulder, V. A. Harmandaris, A. V. Lyulin, N. F. A. van der Vegt, B. Vorselaars, and M. A. J. Michels, *Macromol. Theory Simul.* **17**, 290 (2008).
- [29] V. A. Harmandaris, N. P. Adhikari, N. F. A. van der Vegt, and K. Kremer, *Macromolecules* **39**, 6708 (2006).
- [30] V. A. Harmandaris, D. Reith, N. F. A. van der Vegt, and K. Kremer, *Macromol. Chem. Phys.* **208**, 2109 (2007).
- [31] G. Milano, S. Goudeau, and F. Muller-Plathe, *J. Polym. Sci., B, Polym. Phys.* **43**, 871 (2005).
- [32] S. Izvekov, M. Parrinello, C. J. Burnham, and G. A. Voth, *J. Chem. Phys.* **120**, 10896 (2004).
- [33] F. Ercolessi and J. B. Adams, *Europhys. Lett.* **24**, 2075 (1994).
- [34] S. Izvekov and G. A. Voth, *J. Phys. Chem. B* **109**, 2469 (2005).
- [35] J. P. Ryckaert, G. Ciccotti, and H. J. C. Berendsen, *J. Comput. Phys.* **23**, 327 (1977).
- [36] R. Faller, *Macromolecules* **37**, 1095 (2004).
- [37] P. G. Santangelo and C. M. Roland, *Macromolecules* **31**, 4581 (1998).
- [38] R. Faller, H. Schmitz, O. Biermann, and F. Muller-Plathe, *J. Comput. Chem.* **20**, 1009 (1999).
- [39] J. C. Lagarias, J. A. Reeds, M. H. Wright, and P. E. Wright, *SIAM J. Optim.* **9**, 112 (1998).